DPSPU 81-30-18

CONF-820449--2

WELDING IRIDIUM HEAT-SOURCE CAPSULES FOR SPACE MISSIONS

DPSPU--81-30-18

DE82 020098

W. R. Kanne, Jr.

E. I. du Pont de Nemours and Company
Savannah River Plant
Aiken, South Carolina 29808-0001

March 1982

Paper for presentation at the 63rd Annual Meeting of the American Welding Society, April 26-30, 1982, and for publication in the Welding Journal.

DISCLAIMER

DISCLAIMER

Portions of this document may be illegible in electronic image products. Images are produced from the best available original document.

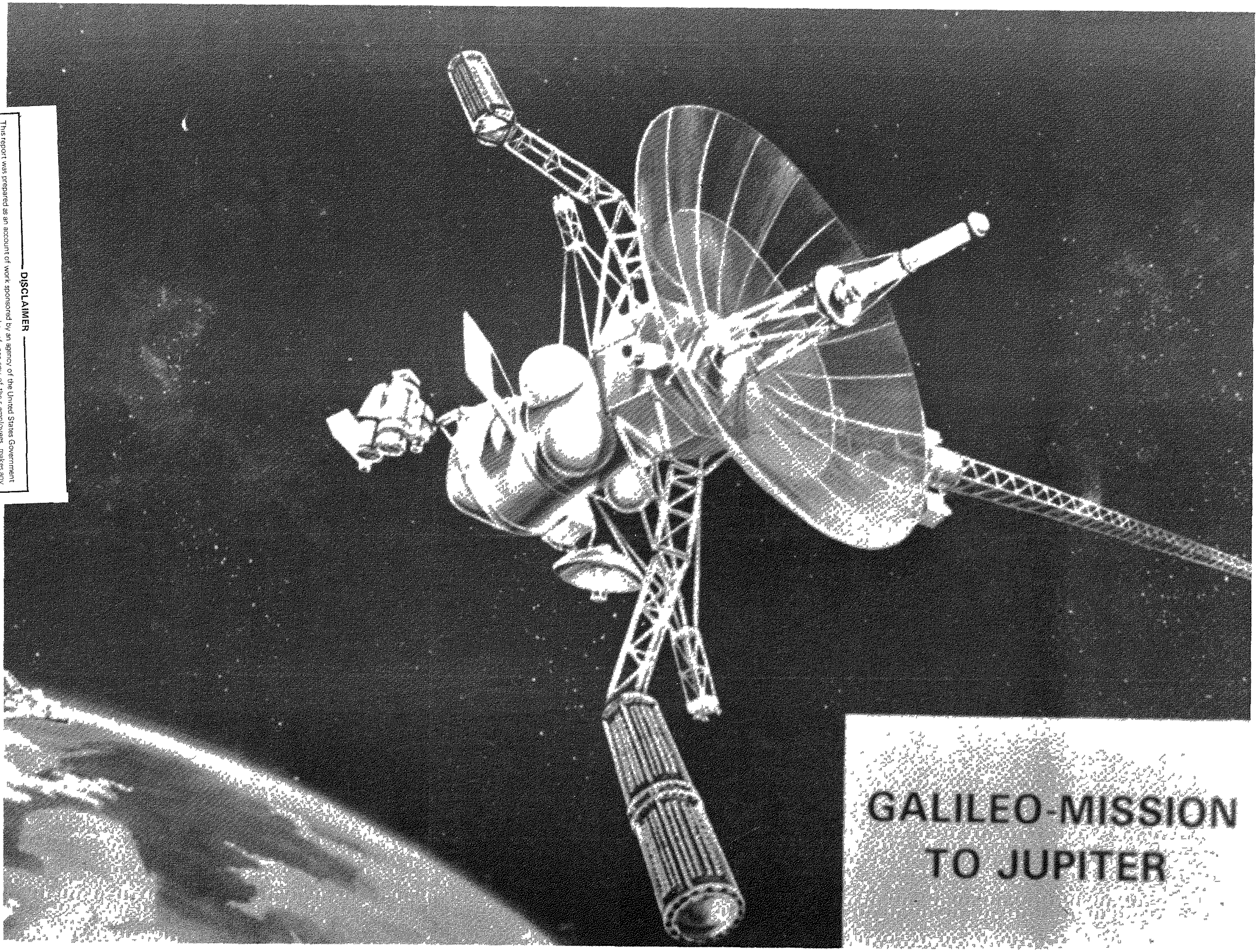

SPACECRAFT WITH THREE HEAT SOURCES ON TWO LONG ARMS

SUBTITLE

A computer controlled gas tungsten arc welding (GTAW) machine is used to encapsulate radioactive $^{238}PuO_2$ in a nonconventional iridium alloy.

INTRODUCTION

Instruments on U.S. interplanetary spacecraft are powered by radioisotope thermoelectric generators. These generators convert decay heat from radioactive plutonium-238 into electrical energy using thermoelectric couples. The plutonium is in the form of an oxide pellet that is hot pressed from powder. Each ceramic pellet produces 62.5 watts of thermal energy. The plutonium must be contained and packaged to prevent accidental release to the environment during possible accident conditions that may occur during launch and ascension through the earth's atmosphere.

Primary containment for the radioactive pellets is provided by a shell of iridum alloy. Iridium is a platinum-group metal that is compatible with plutonium oxide and has good strength and impact resistance at the 1310°C heat source operating temperature. Iridium is unusual in its inertness, high density, and rapid work hardening.

Capsules are thin wall cylindrical shells 0.025 (0.64 mm) in. thick, Fig. 1.

The vent assembly in the end allows the escape of helium gas from radioactive decay but it does not allow escape of PuO_2 fines. The butt weld joint is backed by a 0.005-in. (0.13 mm) thick foil of iridium to minimize the effect of weld heat on the PuO_2 pellet. Completed capsules are loaded into a graphite matrix for final orientation and secondary protection. Pellets are now being fabricated for the Solar Polar and Galileo missions, shown in the lead photo.

THE WELDING OPERATION

Autogeneous gas tungsten arc welding (GTAW) is used to produce a full penetration weld. The weld is made at 30 in./min (12.7 mm/sec) (8 rpm), 83 amperes, and in a helium atmosphere using 20 cfh He - 25% Ar shield gas. Magnetic arc oscillation of 6.5 cycles/sec is used to promote the desired grain structure in the weld (Ref. 1).

The welding operation is carried out remotely in a heavily shielded cell containing manipulator arms and glove ports. Remote operation is required because of the highly toxic nature of the plutonium-238 alpha emitting radioisotope that is being encapsulated.

The welding operation is computer controlled. The fixture, Fig. 2, consists of a turntable, an upper deadweight-loaded positioner, and a horizontally mounted torch. Stepping motors actuate these three functions. Welding current is supplied by a power source with a dual schedule programmer. A small computer controls the stepping motors and coordinates the operation of the fixture with the weld programmer. Instrumentation, Fig. 3, includes a pushbutton control panel for simplified operation by a production operator. Welding parameters and production data can be documented by a computer printout and a fast response current and voltage recorder.

The flexibility of the computer-controlled welding equipment was a significant aid in developing the welding process and in creating an efficient production operation. The computer automatically rotates the capsule through a series of three short tack welds located symmetrically around the capsule. Tack welds maintain alignment of the capsule during the thermal stresses of the full weld. The computer locates the capsule in the proper start position for each weld and strikes the arc three times in succession. The dual welder control allows changing the parameters from the tack to the full weld without resetting the programmer. After the tack welds are inspected, the full weld is automatically sequenced by the computer.

Iridium Welding

An iridium base alloy, "DOP-26," is used for production encapsulation of cylindrical heat sources (Ref. 2). Alloy constituents are a compromise between mechanical properties and weldability. The "DOP-26" alloy contains 0.3 wt % tungsten, 60 ± 30 ppm thorium, and 50 ± 30 ppm aluminum. The addition of small quantities of thorium improves ductility but decreases weldability. Weldability with 60 ppm thorium was demonstrated for bead on plate samples (Ref. 3). Above 100 ppm thorium, the alloy cracks during GTA or EB welding but is weldable with a laser (Ref. 4). Production welding is limited to GTA due to physical and programatic considerations.

External surface appearance of the welds is shown in Fig. 4. The pattern produced by arc oscillation is visible. Weld beadwidths are typically 0.100 in. (2.54 mm) on the external surface and 0.050 in. (1.27 mm) on the inside surface.

Changing welding variables results in dramatic differences in microstructures. Test welds are typically sectioned in face (top surface) and transverse directions. Typical microstructures are shown in Fig. 5 for the production welding speed of 30 in./min (12.7 mm/sec). Lower speeds cause large grains across the weld thickness, Fig. 6A, that are undesirable. Faster speeds cause a weak centerline structure visible in face sections, Fig. 6B. Narrow weld beads where penetration may not be complete have a relatively equiaxed grain structure, Fig. 7A. Wide beads have a coarse colummar structure, Fig. 7B. Typical weld beads are no wider than is necessary to ensure full penetration throughout the weld in all capsules.

Hot Cracking

Cracking at the weld quench was the most significant problem encountered during startup of the welding process. Small underbead cracks up to 0.2 in. (5.08 mm) long developed in the single pass weld bead under the arc taper, Fig. 8A. Cracks were along grain boundaries and did not extend through the capsule wall, Fig. 8B. The largest cracks were along the weld centerline. Cracks aften followed grain boundaries out toward the edge of the weld, Fig. 8C.

Cracks form by a combination of grain boundary liquation and stress. Weld heat at the quench melts thorium phases in the grain boundaries ahead of the weld bead. Thermal stress then produces grain separation. Evidence for this mechanism includes microprobe analysis of crack surface chemistry and surface structure.

- Chemical analysis of material on crack surfaces using a scanning auger microprobe (SAM) shows that thorium is present in concentrations up to 30%. The iridium-thorium phase diagram (Ref. 5) shows a series of eutectics in this region having melting points 300 to 400°C lower than iridium.
- Grain boundary cracks have a characteristic ridge network structure as shown by scanning electron microprobe (SEM) examination, Fig. 9. Networks are present in grain boundaries of the weld underbead, particularly on crack surfaces. They are not found in material remote from the weld. Ridge networks have the appearance of a liquid phase that has pulled apart during the stress of cooling.

Initial attempts to eliminate weld cracks in iridium capsules were unsuccessful. A team of welding experts from five companies was formed to develop process solutions to cracked iridium welds. The team met over a period of three months and developed three approaches:

1) Use of a small backing strip located inside the weld overlap.
2) A stress relief notch with slower welding speed.
3) An increased initial and final taper with slower welding speed.

Initial work showed promise for all three approaches. The third approach showed the most potential for use as a production process. However, an extended program showed that cracks had not been eliminated. Several changes were introduced into the process; they reduced the severity but not the frequency of cracks. Principal changes were a longer final taper and a smaller arc gap (0.035 in. or 0.89 mm). The work on the team approaches showed that the longer final taper was beneficial. The smaller arc gap reduced the beadwidth and improved the microstructure.

WELD QUALIFICATION

Coincident with welding process development, a nondestructive ultrasonic test was developed to inspect finished capsules for weld cracks and other defects. The ultrasonic test configuration, Fig. 10, used a Lamb wave technique. Reliability of this test has been very good. Over 170 capsules have been tested and 38 of them have been destructively examined to compare ultrasonic test results with defects observed by visual and dye-penetrant inspection. All 26 capsules with ultrasonic indications had defects. Cracks were observed in only 2 of 12 capsules having no ultrasonic indications. These two cracks were below the threshold size for detection. The success of the ultrasonic test allowed production to start in spite of a known crack rate of 15% of capsules.

Additional nondestructive inspection of production capsules includes visual examinations, measurements, helium leak testing, and measurement for external surface radioactivity. Capsules must meet specifications for maximum flaw size and have external beadwidths within the range 0.080 to 0.120 in. (2.03 to 3.05 mm). The internal helium atmosphere lends itself to helium leak testing to 10^{-6} atm cc/sec while measurement for external radioactivity serves to indicate any large leaks in the girth weld since radioactivity would leak from the PuO_2 pellet.

Process quality is monitored by destructive examination of the first capsule from each production run of about 10. This examination includes internal bead inspection for penetration and defects. Dye check and metallographic examination are then made to indicate the need for process adjustments in future production runs.

SUMMARY

A remote computer-controlled welding station was developed to encapsulate radioactive PuO_2 in iridium. Weld quench cracking caused an interruption in production of capsules for upcoming space missions. Hot crack sensitivity of the "DOP-26" iridium alloy was associated with low melting constituents in the grain boundaries. The extent of cracking was reduced but could not be eliminated by changes to the welding operation. An ultrasonic test was developed to detect underbead cracks exceeding a threshold size. Production was continued using the ultrasonic test to reject capsules with detectable cracks.

ACKNOWLEDGMENTS

The author gratefully acknowledges the help of the following individuals who made significant contributions to this work: J. W. Kyle and C. O. Williams for experimental assistance; B. J. Eberhard for technical assistance; M. W. Tarpley for ultrasonic test development; W. C. Mosley for analytical studies; M. Gelsie and J. E. Taylor for instrument development; B. D. Sartori and G. D. Teese for mechanical development; C. J. Bearden and S. J. Roberston for metallography; J. D. Scarbrough and D. F. Bickford for technical liason; and the Iridium Welding Committee for technical support. The Welding Committee included representatives from Mound Facility, Los Alamos National Laboratory, Oak Ridge National Laboratory, and Fairchild Industries as well as from the Savannah River Plant.

This paper was prepared in connection with work under contract DE-AC09-76SR00001 with the U.S. Department of Energy.

REFERENCES

1. Coffey, D. L., Jones, W. H., Cartmill, W. B., and Saul, W. A. 1974. Parametric modification of weld microstructure in iridium. Welding Journal 53 (12): 556-s to 568-s.

2. Schaffhauser, A. C. 1976. Isotopic power materials development. Quarterly progress report for period ending December 31, 1976. USDOE report ORNL/TM-5882, June 1977.

3. David, S. A., and Liu, C. T. 1980. Weldability and hot cracking in thorium-doped iridium alloys. Metals Technology 7 (3): 102 to 106.

4. David, S. A., and Liu, C. T. 1980. High-power laser and arc welding of thorium-doped iridium alloys. USDOE report ORNL/TM-7258, May 1980.

5. Moffatt, W. G. December 1979. The handbook of binary phase diagrams: General Electric Co.

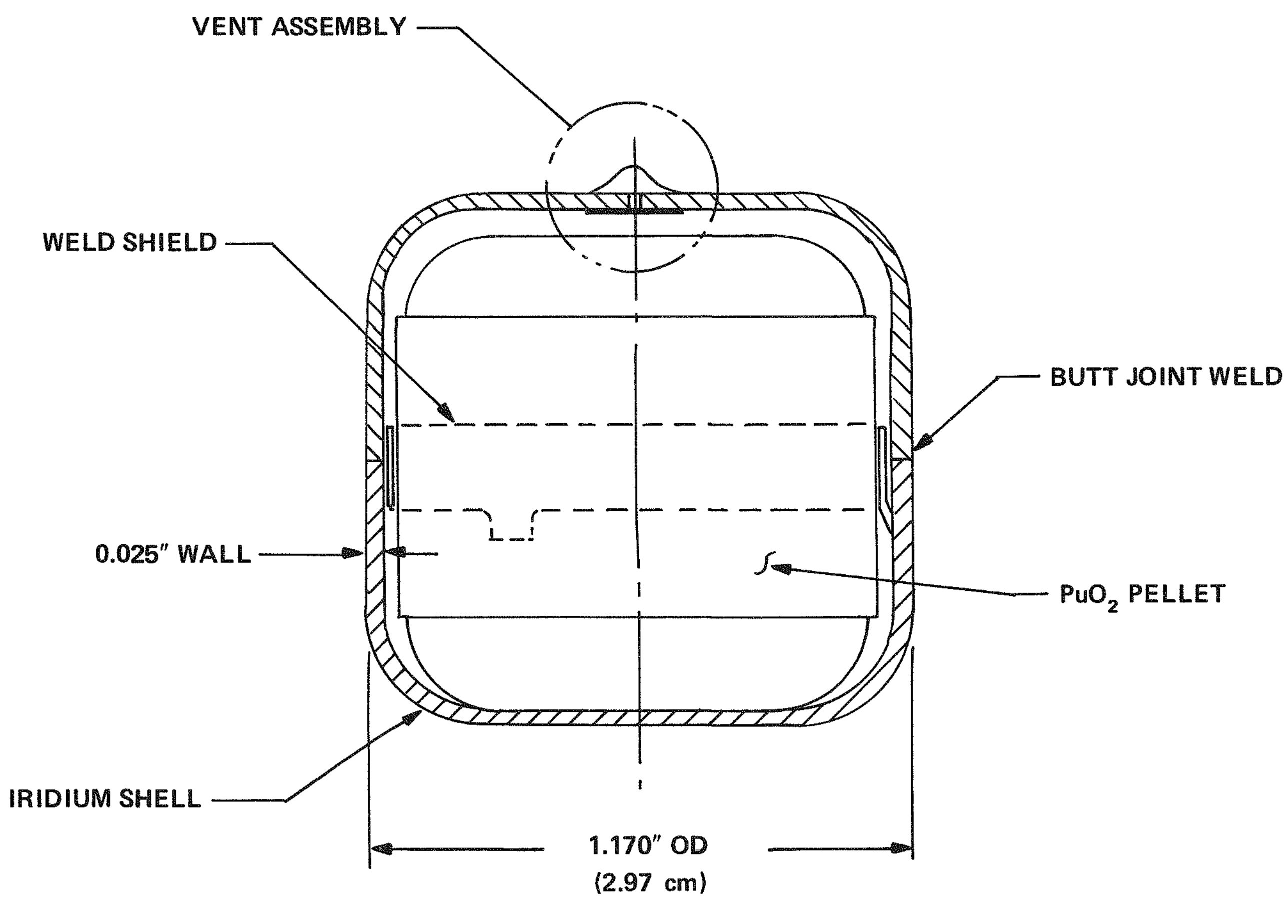

FIG. 1. HEAT SOURCE CAPSULE CONFIGURATION

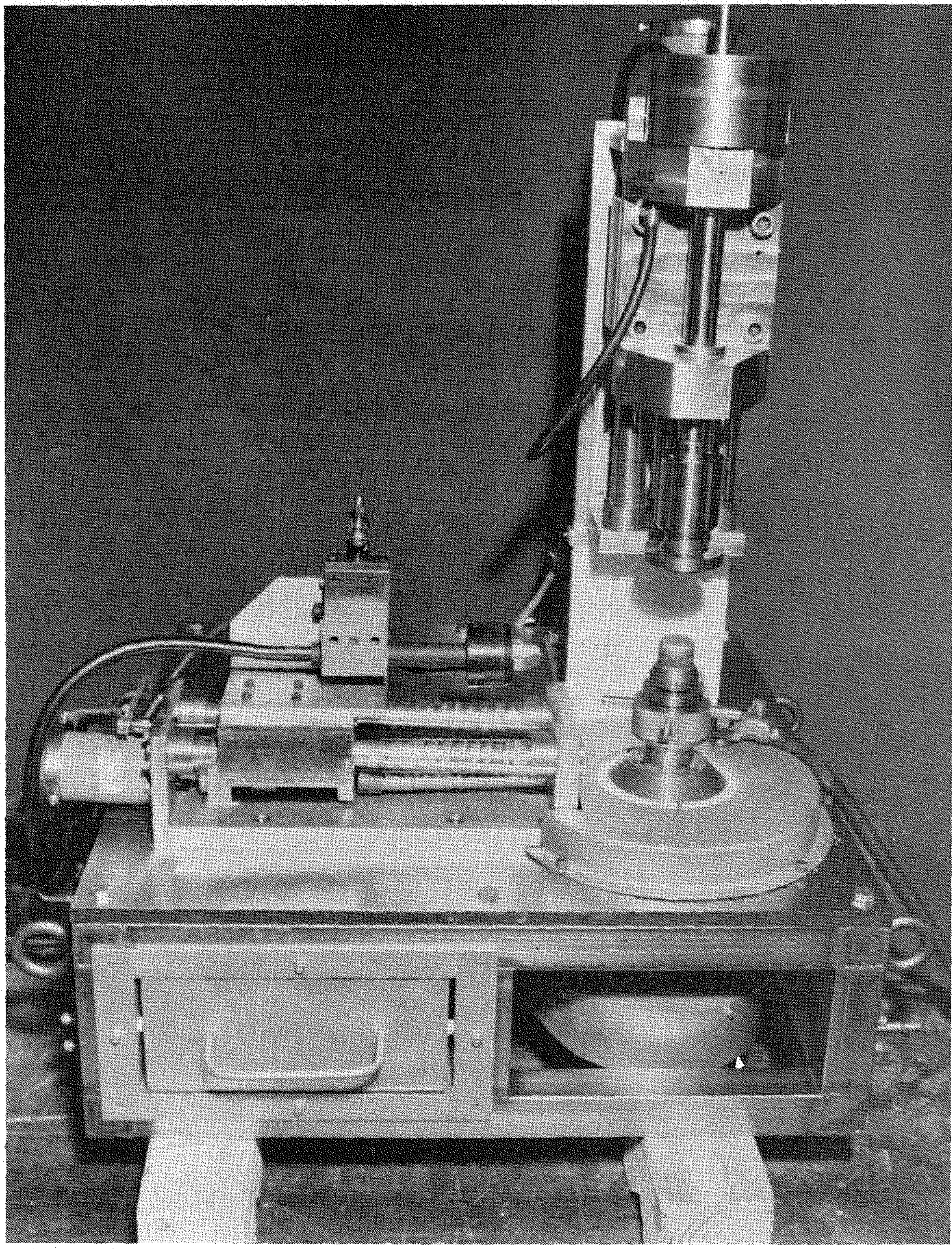

DPSPF 30590-2

FIG. 2. GTA WELDING FIXTURE

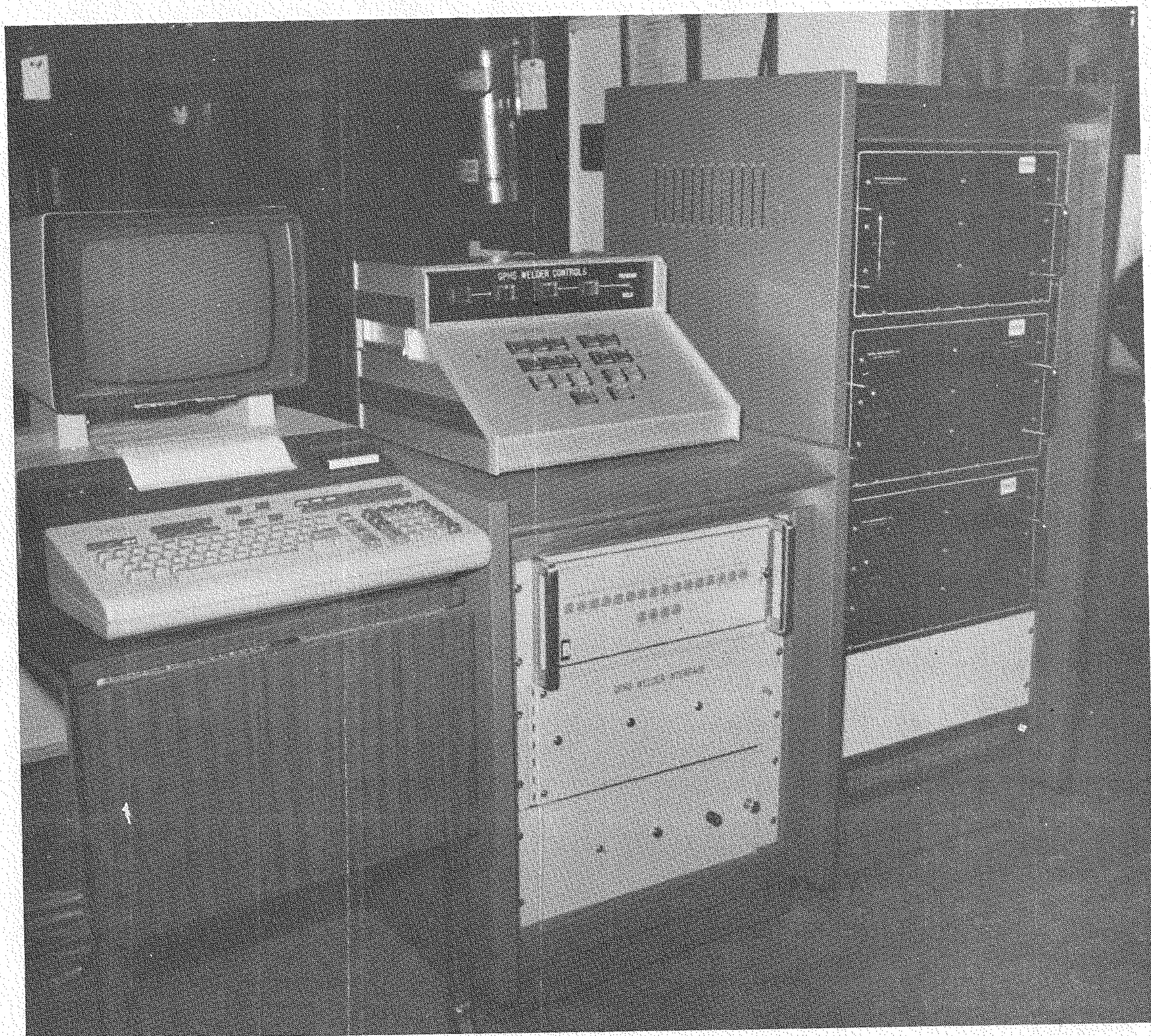

DPSPF 30484-15

FIG. 3. COMPUTER CONTROLS FOR WELDING OPERATION: COMPUTER AT LEFT, OPERATOR CONTROLS AND INTERFACING ELECTRONICS AT CENTER, STEPPING MOTOR DRIVERS AT RIGHT

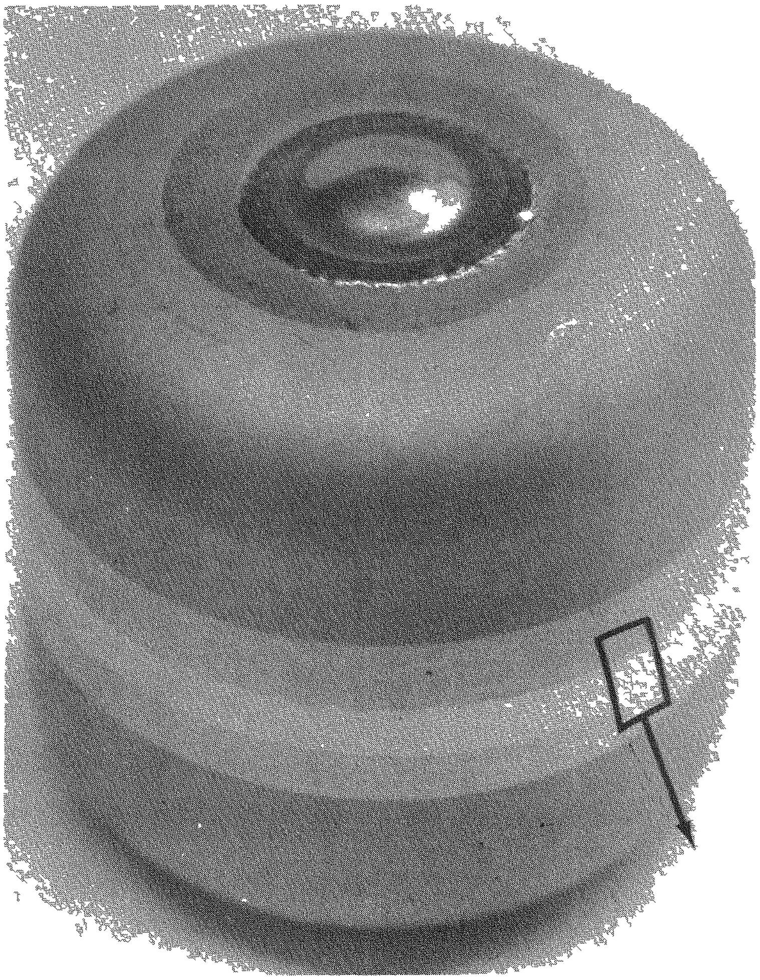

EE 33987-A

EE 33982-A

FIG. 4. WELDED IRIDIUM CAPSULE SHOWING SURFACE PATTERN

EE 36301-A

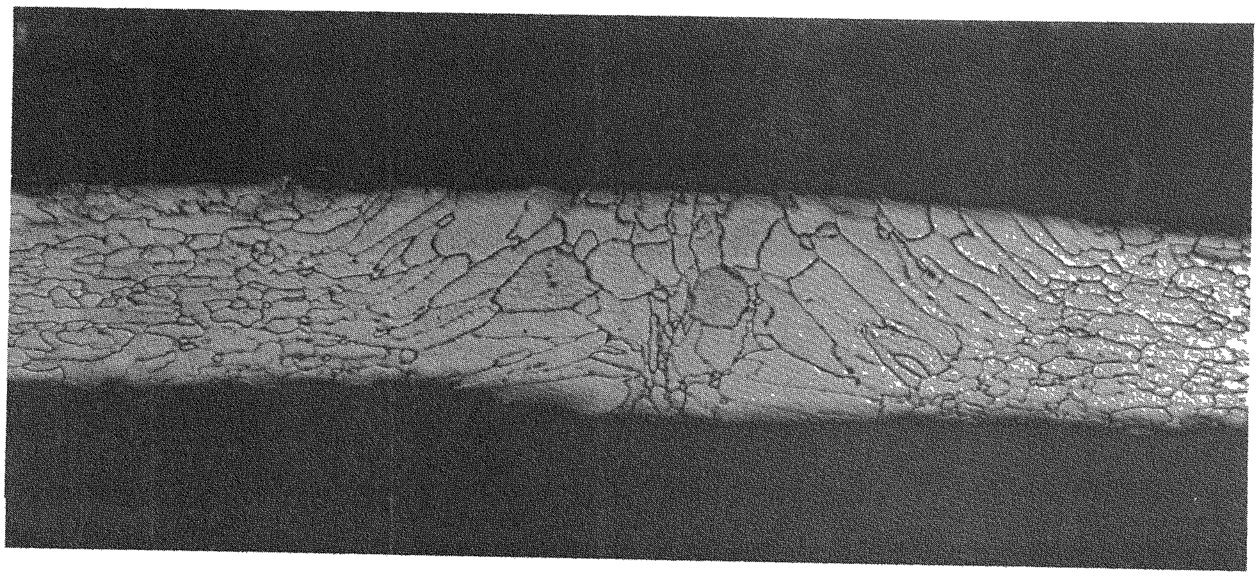

EE 36297-A

FIG. 5. TYPICAL IRIDIUM WELD MICROSTRUCTURES. WELD SPEED 30 IPM.
FACE SECTION (TOP) AND TRANSVERSE SECTION (BOTTOM). X50

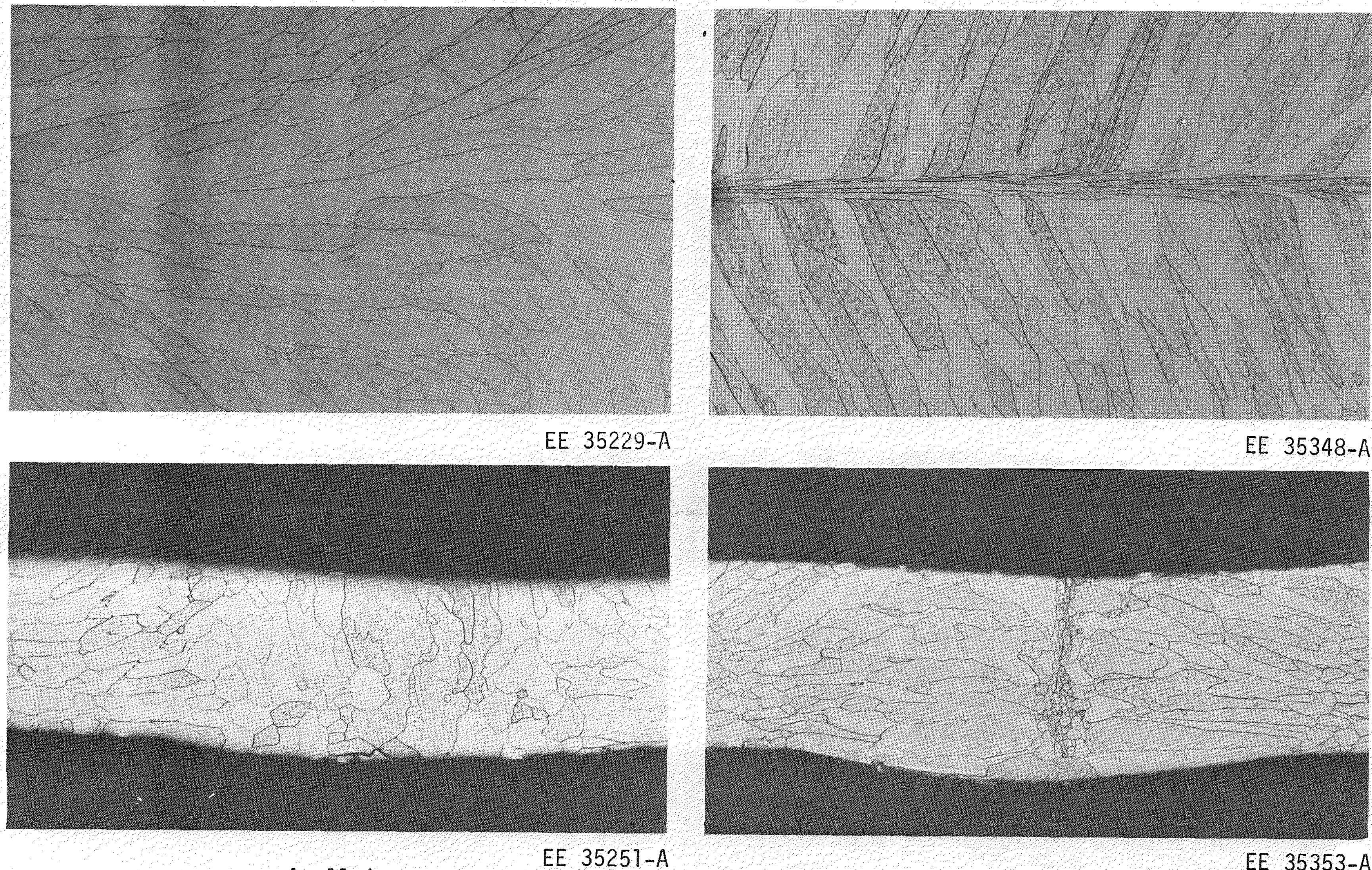

A. 11 ipm

B. 37 ipm

FIG. 6. EFFECT OF WELDING SPEED ON MICROSTRUCTURE. FASTER SPEED RESULTS IN CENTERLINE GRAIN BOUNDARIES IN FACE SECTIONS (TOP). SLOWER SPEED RESULTS IN GRAIN BOUNDARIES THROUGH WALL IN TRANSVERSE SECTIONS (BOTTOM). X50

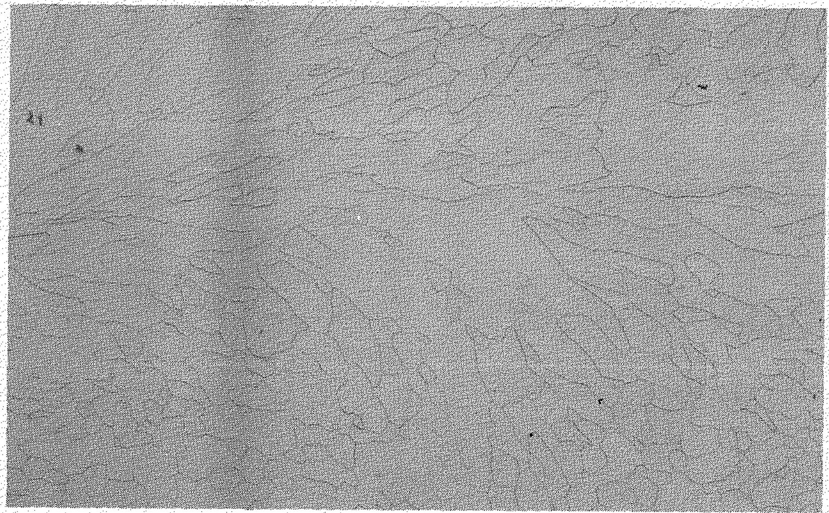

EE 35657-A

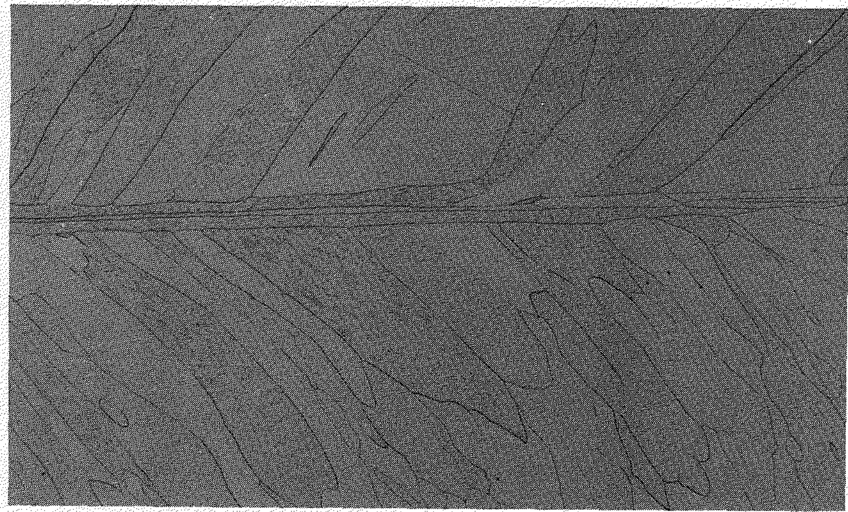

EE 35224-A

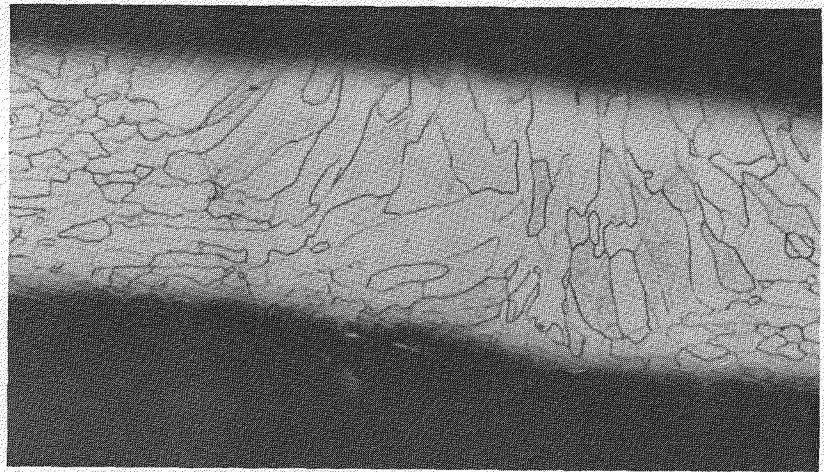

EE 35646-A

A. 0.080" (0.2 cm) BEADWIDTH

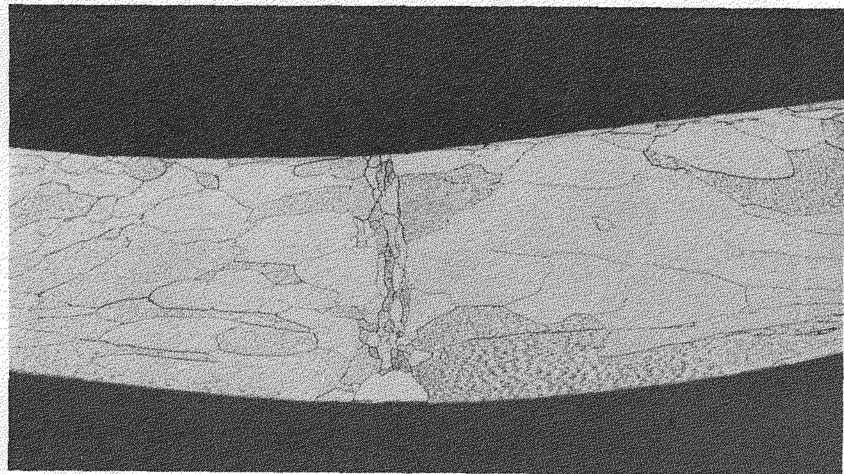

EE 35272-A

B. 0.120" (0.3 cm) BEADWIDTH

FIG. 7. EFFECT OF WELD HEAT ON MICROSTRUCTURE. NARROW BEADS (A) RESULT IN A RELATIVELY EQUIAXED GRAIN STRUCTURE WHILE WIDE BEADS (B) RESULT IN A COLUMNAR STRUCTURE. X50

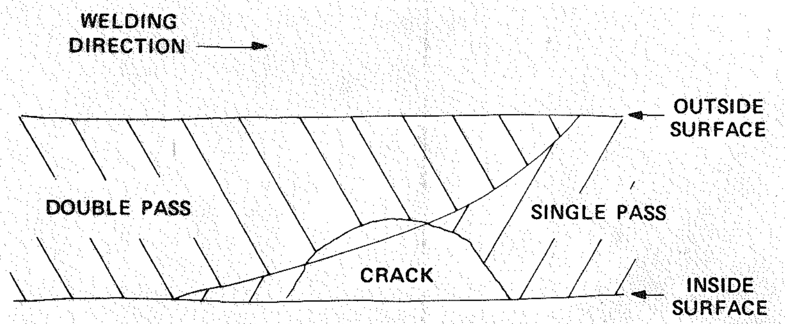

A. SCHEMATIC OF LONGITUDINAL SECTION SHOWING TYPICAL CRACK LOCATION

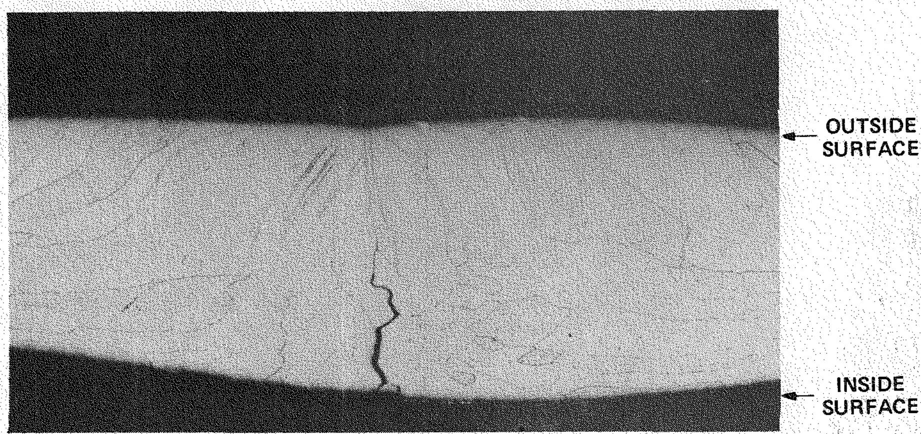

EE 4669-F

B. TRANSVERSE METALLOGRAPHIC SECTION OF TYPICAL CRACK. X50

SRL-SEM-1344

C. SEM PHOTO OF CRACKS ON INSIDE WELD SURFACE, X80

FIG. 8. TYPICAL CRACKS IN WELD UNDERBEAD

EE 37292-A

FIG. 9. RIDGE NETWORKS ON GRAIN FACETS OF CRACK. X3,000

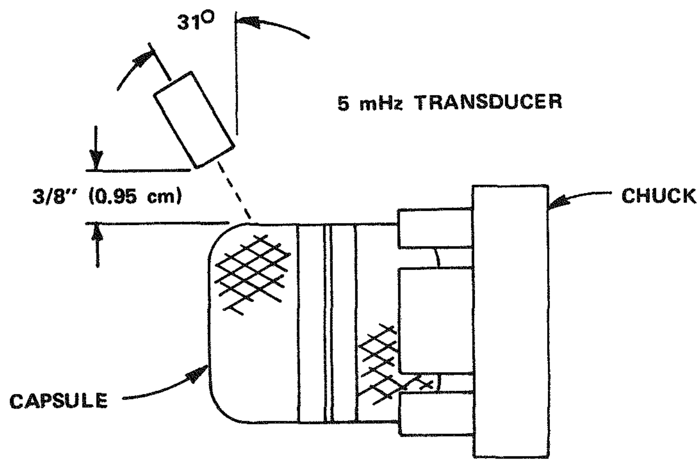

FIG. 10. ULTRASONIC TEST CONFIGURATION

Do not micro-film

DISTRIBUTION

AED Wilmington

J. E. Conaway
F. E. Kruesi
J. F. Proctor
Wilm File

Savannah River Laboratory

S. Mirshak
S. D. Harris, Jr.
R. L. Folger, 773-A
J. P. Howell, 773-A
W. C. Mosley, 773-A
E. F. Sturken, 773-A
D. F. Bickford, 773-A

Savannah River Plant

J. T. Granaghan-
T. Hendrick, 703-A
H. J. Groh, 703-A
A. H. Peters, 703-A
D. L. McIntosh, 703-A
E. O. Kiger, 703-A
G. W. Wilds, 703-A
M. M. Anderson, 703-A
J. K. Brown, 704-F
G. L. Albert, 235-F
M. R. Beckmeyer, 235-F
D. C. Nichols, 704-F
L. P. Fernandez, 704-F
B. K. Roberts, 235-F
J. D. Scarbrough, 235-F
R. F. Mittelberg, 723-7A
R. F. Philipp, 322-M
C. J. Bearden, 221-H
S. J. Robertson, 313-M
M. E. Bowman, 723-A
H. R. Reeve, 723-3A
T. H. Burke, 723-6A
M. W. Tarpley, 723-A
K. W. MacMurdo, 723-A
R. W. Clark, 723-A
J. E. Taylor, 723-A
M. Gelsie, 723-A
J. M. Ferrell, 723-3A
G. D. Teese, 703-3A
B. D. Sartori, 105-K
M. D. Buxton, 723-A
E. C. Speed, 723-A
B. J. Eberhard, 723-A
J. R. Harpring, 723-A
J. W. Kyle, 723-A
C. O. Williams, 723-A
W. R. Kanne, Jr., 723-A (5)
TIS File, 773-A (12)
TS File, 703-A
R&AS Extra Copy File, 703-A
R&AS Vital Records File, 703-A
R&AS Record Copy File, 703-A